

# Crystallization history of sector-zoned microcline megacrysts from the Godani Valley pluton, Nigeria

DAVID VANIMAN<sup>1</sup>

Board of Earth Sciences, University of California, Santa Cruz, California 95064

**SUMMARY.** Sector-zoning is brought out by mineral inclusions (plagioclase, biotite, hornblende, sphene, and apatite) in 2 to 5 cm microcline megacrysts of the Godani Valley pluton, Nigeria. The inclusions are concentrated in the megacryst rims beneath the faces  $\{110\}$  and  $\{20\bar{1}\}$ ; the megacryst cores are not sector-zoned. Comparison with other occurrences (Portugal and Czechoslovakia) shows that this type of sector-zoning is not controlled by growth rate. Chemical sector-zoning does not occur in the Godani megacrysts. Growth from magma is proposed, with preference for inclusions on faces at a high angle to the feldspar *a*-chain. A superficially similar type of sector-zoning occurs in microcline megacrysts of both pluton and wall rock at Papoose Flat, California, suggesting that this feature can be generated either by growth from magma or by replacement.

**SECTOR-ZONING** is reflected in the distribution of mineral inclusions within microcline megacrysts from a pluton in the valley around Godani Station, 50 km SW of the city of Kaduna, Nigeria (fig. 1). This pluton contains 2-14% megacrysts by volume but has a constant total abundance of megacryst plus groundmass microcline (c. 22%). Sector-zoning was found in megacrysts from all localities except site 46 (fig. 1), which has the greatest abundance of megacrysts (14%).

In general the 2-5 cm euhedral megacrysts are randomly distributed, but they also occur in elongate aggregates parallel to foliation trends or in clusters around cognate mafic clots. Sector-zoning appears within euhedral megacrysts in such occurrences but is not observed in large patches (c. 1 cm<sup>2</sup>) of anhedral microcline within the mafic clots.

Sector-zoning appears in the megacryst rims where mineral inclusions are concentrated beneath the faces  $\{110\}$  and  $\{20\bar{1}\}$ . Inclusions of oligoclase,

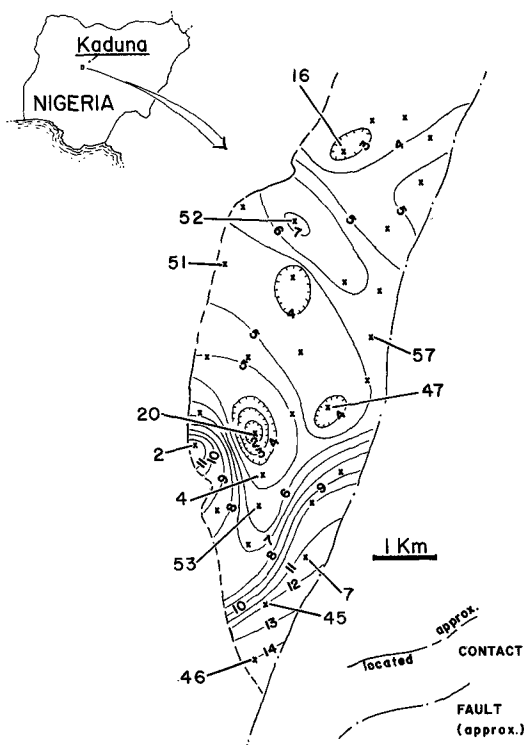


FIG. 1. Contour map of percentage megacryst abundance within the Godani Valley pluton. Sampled stations are indicated (x), and stations discussed in the text are numbered.

biotite, hastingsitic hornblende, apatite, and sphene occur throughout each megacryst. Quartz inclusions appear only in the megacryst cores, which are not sector-zoned. The elongate and tabular minerals are oriented parallel to the megacryst faces (ref. Godani specimen, fig. 2).

<sup>1</sup> Present address: Department of Earth and Space Sciences, State University of New York, Stony Brook, New York 11794.

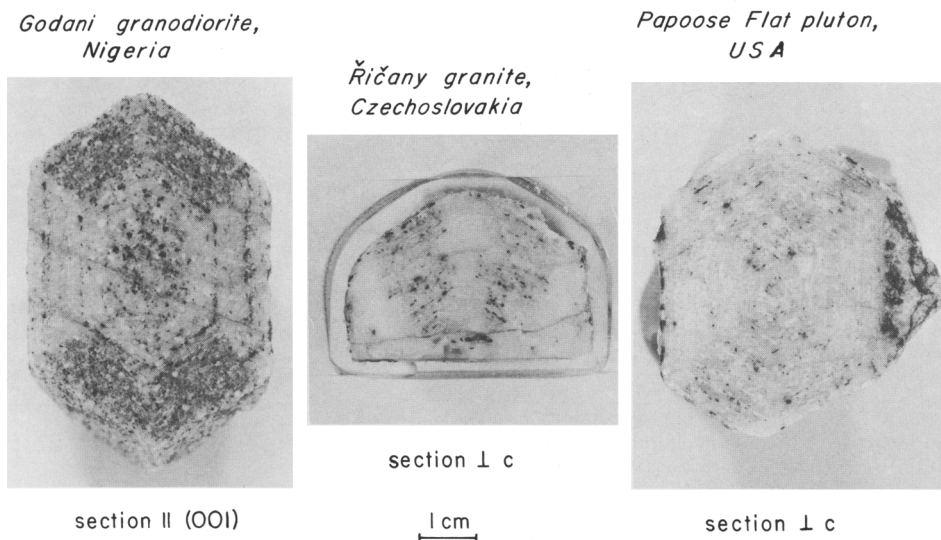


FIG. 2. Photographs of centred sections through sector-zoned megacrysts; Czechoslovakian specimen donated by Dr. E. Piveč.

A magmatic origin for the host pluton is inferred from cross-cutting contacts along the western margin. Saturated magma relationships are shown by analyses plotted in the systems Ab-Or-Qz and Ab-Or-An-Qz. This study will show that the megacrysts too must be magmatic.

**Methods.** Chemical compositions of minerals were obtained on an ARL electron microprobe. The empirical methods of Bence and Albee (1968) were used for correction of data. Plagioclase, biotite, and hornblende were analysed both inside the microcline megacrysts and within the groundmass (data available on request). Analyses of megacryst and groundmass microcline are listed in Table I (p. M41).

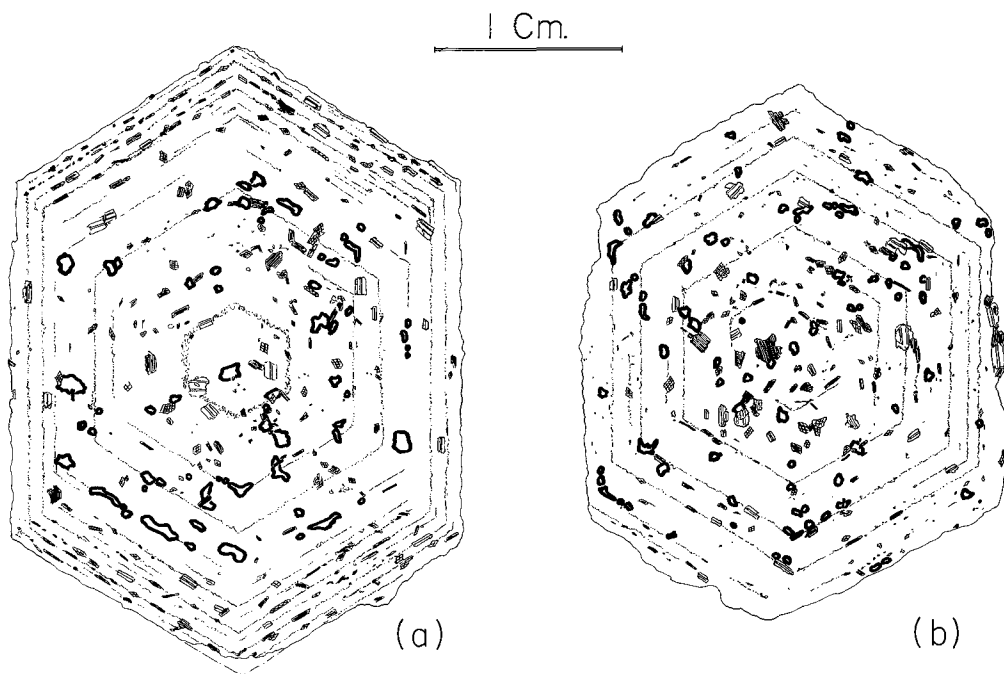
Megacrysts and groundmass were analysed by X-ray fluorescence. Groundmass analyses were obtained from fresh samples trimmed of megacrysts. Seven megacrysts were cut into core, inclusion-rich rim, and inclusion-poor rim for analysis. Fusion pellets of specimen-NaNO<sub>3</sub>-spectroflux were used for all elements except Na, Ba, Rb, and Sr, for which pressed-powder pellets were used. Analyses are listed in Table II (p. M42).

In order to determine the variation in morphology during crystal growth, fifteen specimens were cut in half parallel to (010) and measured ring-by-ring with a binocular microscope (ref. fig. 4). Thick (*c.* 0.5 mm) centred slices perpendicular to the *c*-axis were also cut from megacrysts from each of the thirty-one sample localities and measured by microscope in transmitted light (ref. fig. 5).

Microcline structural states were investigated using the X-ray powder diffraction methods of Wright and Stewart (1968) and Stewart and Wright (1974). X-ray powder diffraction scans of 45 core, inclusion-rich rim, and inclusion-poor rim portions of five megacrysts were made with Cu radiation on a monochromator-fitted goniometer. Three oscillations from 19° to 59° 2θ at ½° per minute were made for each analysis. Annealed CaF<sub>2</sub> was used as an internal standard. Cell parameter refinements were made using the method of Evans *et al.* (1963).

**Internal geometry: changing megacryst habit with onset of sector-zoning.** Mineral inclusions mark concentric growth rings in the Godani megacrysts. The concentric shapes outlined by continuous layers of inclusions record the megacryst morphology during each particular growth episode. Measurements of these shapes show that the crystal morphology changes with the onset of sector-zoning in megacryst rims.

Inclusion-defined crystal shapes on sections cut parallel to (010) were measured for fifteen crystals from eleven localities. Five (010) sections from separate localities are shown in fig. 4. The four (010) sections of sector-zoned megacrysts (2, 20, 51, 57) show a discontinuity in shape where sector-zoning appears in the crystal rims. Although still concentric with previous growth, crystal rims are more *a*-elongate. Specimens from site 46, where sector-zoning is not developed in the megacrysts, show no variation in morphology throughout their growth history.




note:  → quartz inclusions are indicated by heavy outline

FIG. 3. (a) Sector-zoned crystal from site 51; note absence of quartz inclusions in the megacryst rim. (b) Crystal from site 46, without sector-zoning; note presence of quartz inclusions throughout. Sections are  $\perp c$ .

Fig. 5 shows the morphological dimensions  $b$  and  $a'$ , where  $a'$  corresponds to the projection of morphological  $a$  on to the section perpendicular to the  $c$  axis. There is a distinct difference in the  $a':b$  ratios of the core and rim portions. This ratio averages  $(1.20 \pm 0.03):1$  for cores and  $(1.42 \pm 0.02):1$  for sector-zoned rims. Megacrysts from site 46, which lack sector-zoning, have the  $a':b$  ratio of  $1.20:1$  throughout.

These changes in morphology suggest faster growth of the faces  $\{110\}$  and  $\{20\bar{1}\}$  during sector-zoning. By itself this observation would indicate a growth-rate control of this type of sector-zoning. However, Schermerhorn (1956) and Piveč (1969) have found the same orientation of sector-zoning in  $c$ -elongate microcline; in these occurrences growth rate is not the controlling factor in the inclusion of groundmass minerals.

**Megacryst chemistry.** Microprobe analyses of megacrysts show little compositional variation. Table I, p. M41 lists eighteen representative analyses from megacrysts and groundmass microcline. The megacryst analyses are from the cores, the inclusion-rich rim sectors, and the inclusion-poor rim sectors of individual crystals from five of the localities

shown in fig. 1. There is a slight variation in  $\text{BaAl}_2\text{Si}_2\text{O}_8$  (celsian) content between rim sectors of any one site, and a slight decrease in celsian content from core to rim. However, groundmass microcline is significantly more potassic and has lower celsian content. Fig. 6 shows that the celsian content is always less in groundmass microcline than in microcline megacrysts. The dividing point between groundmass and megacryst microcline is notably constant at 0.85 mol. % celsian throughout the pluton. Several studies have shown that Ba tends to concentrate in early-crystallizing K-feldspar, leaving the later-precipitating K-feldspars depleted (Ofstedal, 1959; Taylor and Heier, 1960; and Kerrick, 1969).

**Mappable variation of 131-131 peak separation within the pluton.** One expects a diffraction symmetry consistent with Al-Si distribution: triclinic symmetry with highly ordered Al-Si distribution and monoclinic symmetry with disordered intermediate ('orthoclase') to sanidine structures. However, a crystal twinned on the unit-cell scale can have a monoclinic diffraction pattern regardless of Al-Si distribution; in this case the sub-microscopic twin relation may create an orthogonal 'average' of

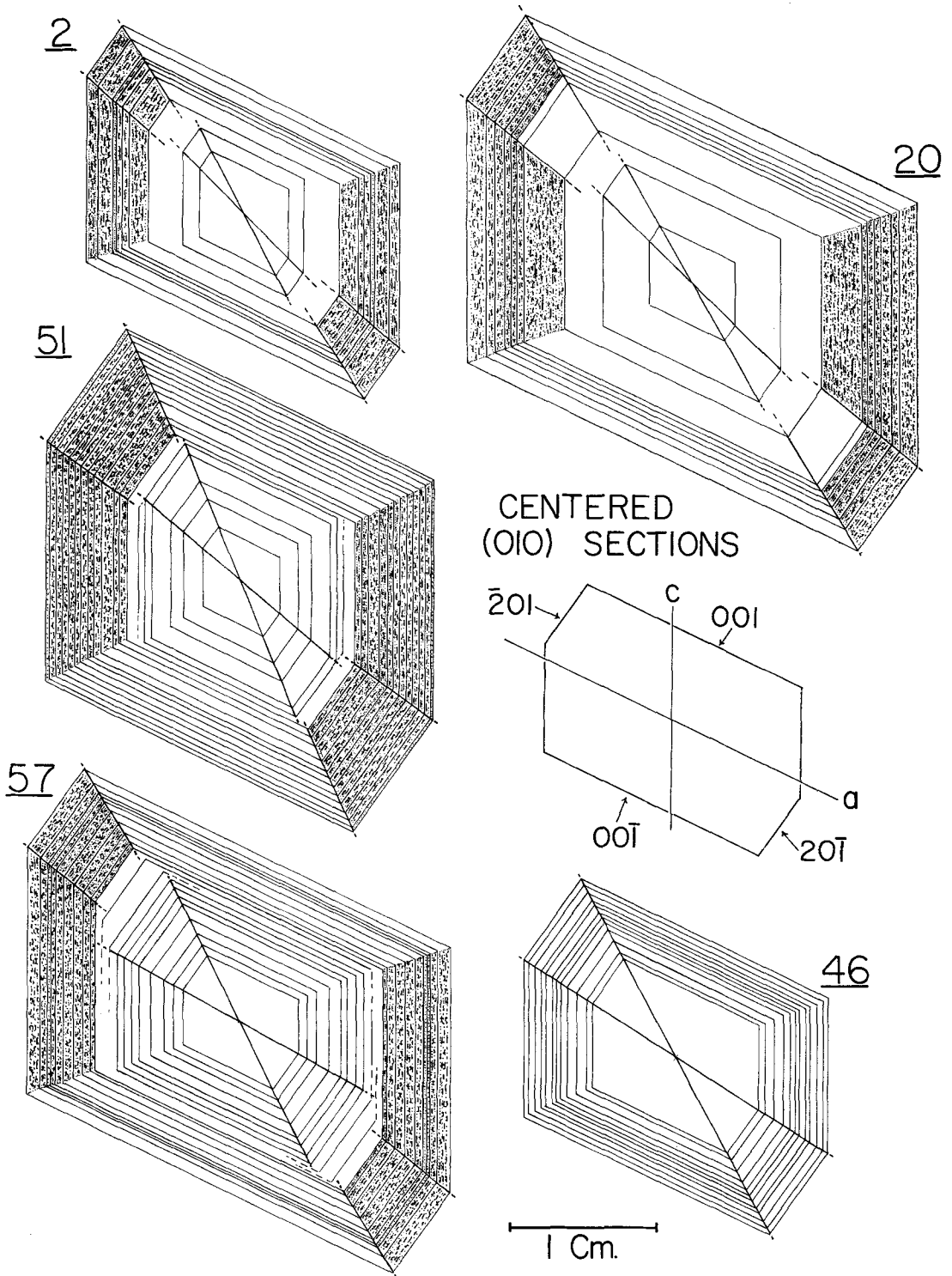


FIG. 4. Measured growth on (010) megacryst sections. The specimens are from five localities numbered in fig. 1. All growth shapes have the same symmetrical centre. Zones of abundant inclusions in the rims are stippled. Note that sector-zoning does not occur in the specimen from site 46. A change in crystal shape is seen in the transition from core to sector-zoned rim in crystals from the other four sites. This change is due to elongation along the *a*-axis, as discussed in the text.

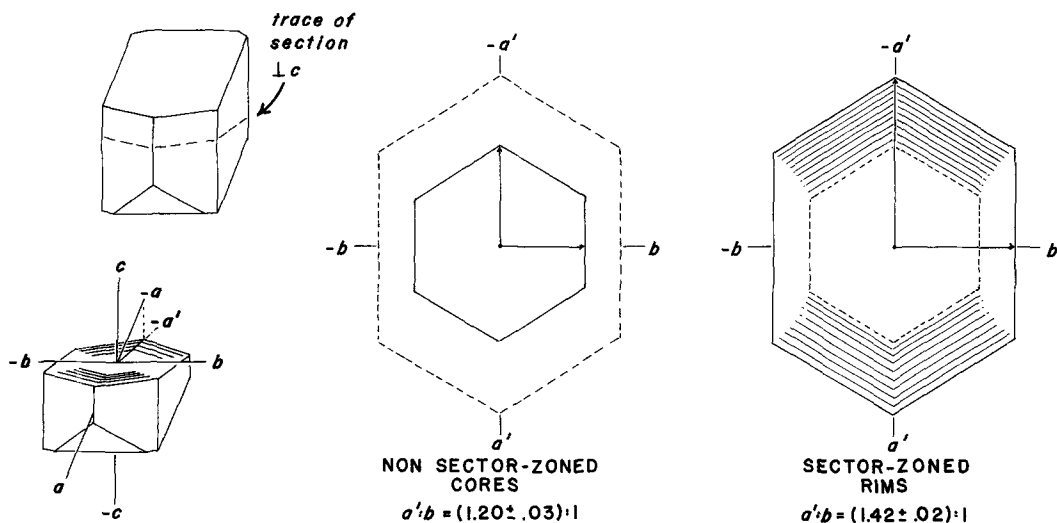


FIG. 5. The different shape of cores and rims in megacryst sections perpendicular to *c*. The ratio  $a' : b$  is used to measure variation. Variation in *c* is not systematic (see text).

the  $\alpha$  and  $\gamma$  cell angles (Laves and Goldsmith, 1961). This apparently occurs in the Godani megacrysts, where the Al-Si distribution is highly ordered but the powdered specimen and single-crystal diffraction patterns often have a pronounced monoclinic symmetry.

There is no sectoral control over the presence of monoclinic symmetry within single megacrysts, but all megacrysts within a single locality have either a single 'monoclinic' (131) diffraction peak or triclinic (131-131) peak separation. This feature can be mapped across the pluton (fig. 7). Separation

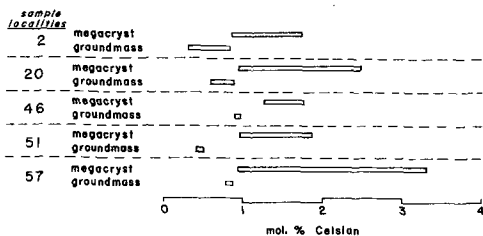


FIG. 6. Range of celsian content in groundmass and megacryst microcline from five localities of fig. 1. Groundmass microcline is always lower in celsian, and the ranges of megacryst and groundmass celsian content do not overlap. Data are from microprobe analyses.

MAP OF 131-131 PEAK SPLITTING WITHIN THE GODANI PLUTON

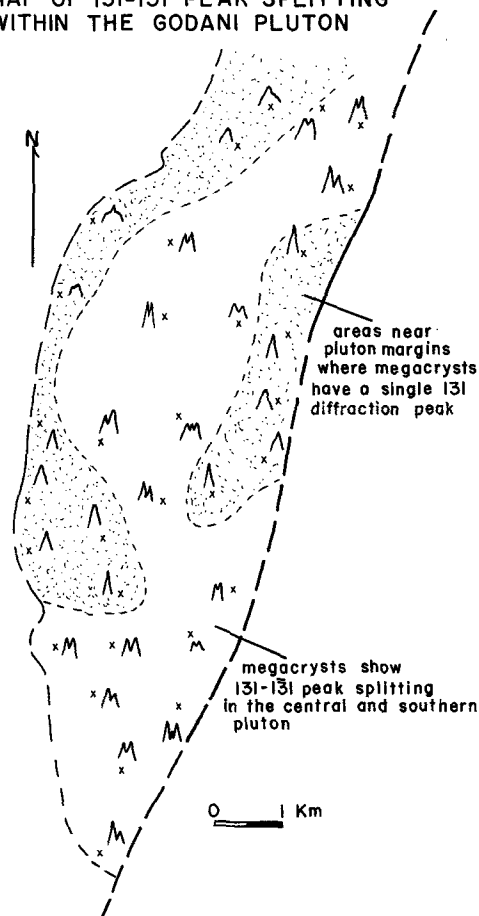


FIG. 7 (right). Map of triclinic and monoclinic powder-diffraction features within the Godani Valley pluton. The shape of 131 (and 131) diffraction peaks is shown at each sample locality.

of 131 and 131 peaks in the diffraction patterns is found only in the central and southern pluton. The southern edge of the pluton is in contact with mobilized gneisses of a deeper (and hotter) tectonic regime than the schists along the northern contact and the central pluton must have retained heat longer than the chilled contacts did. Thus the southern contacts and the central pluton may have cooled more slowly than the northern contact zone. The monoclinic symmetry in megacrysts along the northern contact is evidence of a more chilled magmatic margin, along which some elements of monoclinic K-feldspar symmetry were 'quenched in' at high temperature.

*Crystallization history of Godani megacrysts.* Whole-rock compositions calculated from megacryst and groundmass XRF analyses (Table II, p. M42) are plotted in fig. 8. Within the Ab-Or-Qz ternary system these compositions fall near the ternary minimum at 5 kb  $P_{H_2O}$  (Luth *et al.*, 1964). The absence of quartz inclusions in megacryst rims was described above (fig. 3); this lack of quartz is also seen in the normative compositions calculated for megacryst rims (fig. 8). A gap in quartz

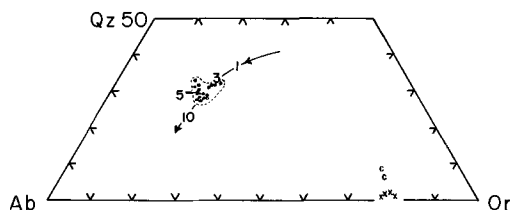


FIG. 8. Normative Ab-Or-Qz; whole rock compositions are shown as circles and megacryst compositions as symbols  $x$ ,  $c$ . The path of the ternary minimum with increase of  $P_{H_2O}$  is shown with 1, 3, 5, and 10 Kb positions marked (ref. Luth *et al.*, 1964). Note the absence of normative quartz from megacryst rims ( $x$ ) and presence of normative quartz in cores ( $c$ ).

crystallization history can be explained within the Ab-Or-An-Qz system. In this system crystallization would progress as shown in fig. 9a, beginning near the plagioclase-quartz quaternary divariant surface. The initial composition  $L$  will be assumed to be slightly within the plagioclase primary field. As plagioclase precipitates and reacts, the composition of the liquid will change along the path  $L-L^1$ . Upon reaching  $L^1$  the fluid will begin to precipitate quartz, and the path of liquid variation will be  $L^1-L^2$  until a composition on the quaternary univariant line  $e-b$  is reached. Once the line  $e-b$  is intercepted, the three phases quartz-plagioclase-potassium-feldspar will precipitate simultaneously as the liquid composition changes from  $L^2$  toward

$e$  along the line  $e-b$ . The simultaneous precipitation of plagioclase and quartz with microcline corresponds to the inclusions observed in the cores of the Godani megacrysts.

Loss of quartz inclusions in the megacryst rims requires that the path of liquid composition leave the univariant line  $e-b$ . Luth (1969) has shown that a decrease in pressure results in displacement of the quartz-alkali-feldspar saturation surface towards the quartz apex of the Ab-Or-Qz system. This is true for dry, water-undersaturated, and water-saturated systems. Presnall and Bateman (1973) have extended Luth's conclusions to the system Ab-Or-An-Qz; in this system the divariant surface  $a-b-c-d-e$  (fig. 9) is displaced towards the quartz apex with any decrease in pressure. Returning to liquid composition  $L^3$  in fig. 9a, it is evident that any decrease in pressure with de-gassing or upward intrusive movement will place  $L^3$  within the primary field of plagioclase ( $e'-b'-c'-d'-Ab-An-g'-f'$ ; fig. 9b). Only plagioclase will crystallize along the path  $L^3-L^4$ , followed by simultaneous precipitation of plagioclase and potassium feldspar when the liquid composition meets the surface  $e'-b'-g'-f'$  at  $L^4$ . The new crystallization path  $L^3-L^4$  may briefly resorb part of the megacryst growth and some groundmass quartz. When K-feldspar crystallization recommences along the path  $L^4-L^5$ , it will be without the simultaneous precipitation of quartz. This coincides with the absence of quartz inclusions within the sector-zoned rims of Godani megacrysts. Crystallization of quartz will not resume until the fluid composition reaches the displaced  $e'-b'$  boundary at  $L^5$ . Further crystallization must be along the line  $e'-b'$ , from  $L^5$  toward  $e'$ . This would continue until the liquid disappears.

There must have been a considerable amount of crystallization along the liquidus path  $L^5-e'$  after megacryst growth. Megacryst microcline accounts for at most 65% of the normative Or component in the average Godani granodiorite. Post-megacryst K-feldspar crystallization is concentrated in small 0.25 mm anhedral grains around larger 2-5 mm subhedral to euhedral plagioclase crystals. The outer surfaces of the microcline megacrysts continued to grow along with the final episode of groundmass quartz and plagioclase precipitation, and small 0.1 mm round quartz inclusions are found within the outer megacryst surface.

*Crystallographic control of the sectoral preference for inclusions in magmatic K-feldspar.* Kastner and Waldbaum (1968) and Bahat (1974) explained sectoral preference for inclusions in feldspar by a growth-rate mechanism. Both described plagioclase morphologies in which faces that grew faster accepted abundant inclusions. This might seem to be the explanation of sectoral features

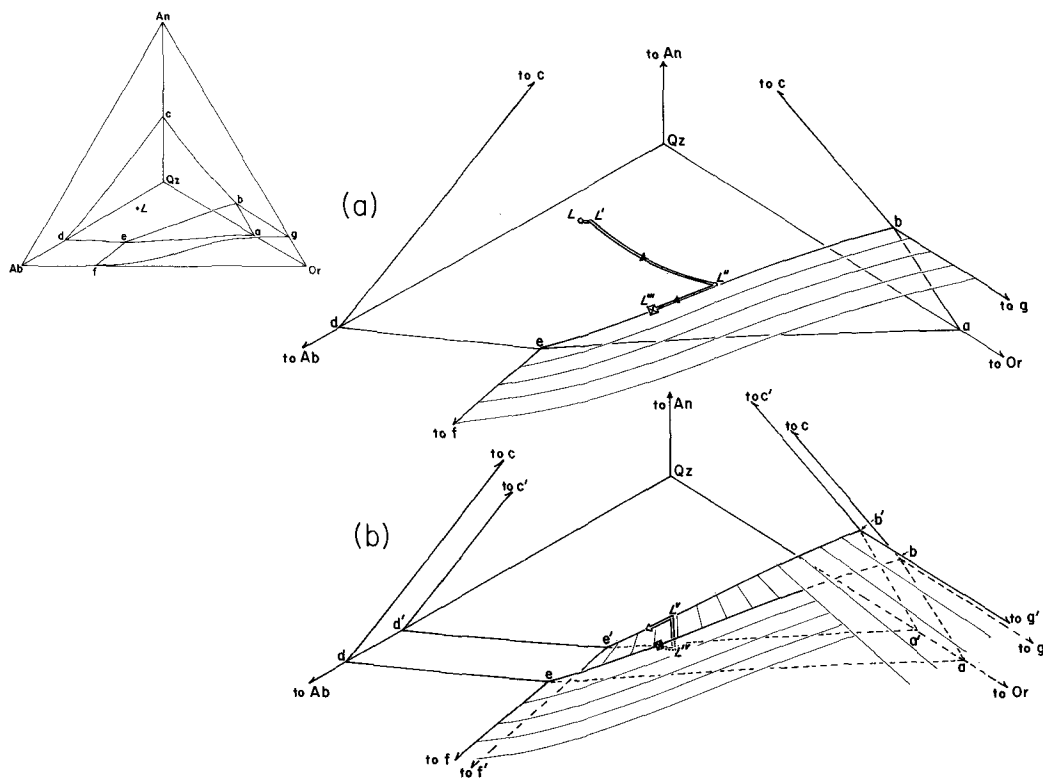


FIG. 9. Schematic phase relations in the system (Ab-Or-An-Qz) after Carmichael (1963) and Presnall and Bateman (1973). The point  $L$  = average whole-rock composition of the Godani pluton. Liquid fractionation paths are: (a) within the plagioclase field ( $L-L'$ ), on the plagioclase-quartz-divariant saturation surface ( $L-L''$ ), and on the plagioclase-quartz-potassium-feldspar univariant saturation line ( $L''-L'''$ ). The plagioclase-potassium-feldspar divariant surface ( $b-e-f-g$ ) is striped. (b) with decrease in pressure the divariant surface  $b-e-f-g$  is displaced to  $b'-e'-f'-g'$ . The new divariant surface is indicated by striping at right angles to the former one, where visible in this view. Starting from point  $L''$  on the former univariant line  $e-b$ , the fractionation path is once again within the plagioclase field ( $L''-L'''$ ), on the plagioclase-potassium-feldspar divariant surface ( $L''-L'''$ ), and finally between  $L''$  and  $e'$  along the displaced univariant line  $e'-b'$ . The absence of quartz inclusions in sector-zoned megacryst rims implies that sector-zoning occurred along the path  $L''-L'''$  on the plagioclase-potassium-feldspar liquidus surface, without simultaneous quartz crystallization.

in the Godani megacrysts, where inclusions are picked up on the  $\{110\}$  and  $\{20\bar{1}\}$  faces as their growth rates accelerated. Evidence from the Godani megacrysts alone argues for a simple growth-rate mechanism. However, this explanation fails to explain the megacrysts described by Schermerhorn (1956) and Piveç (1969), which are elongate parallel to  $c$  yet contain abundant inclusions on the growth forms  $\{110\}$ , which lie parallel to the direction of most rapid growth.

Instead of growth-rate control, a crystallographic control is indicated by the consistent accumulation of groundmass inclusions on faces that are at a high angle to the  $a$ -axis. These are the faces  $\{110\}$ , described by Schermerhorn (1956) and Piveç (1969)

and seen in the Godani megacrysts, and on the face  $\{20\bar{1}\}$  described in this paper. These faces accumulate inclusions by some mechanism that does not operate on faces parallel to the  $a$ -axis.

'Double crankshaft' chains of tetrahedral units parallel to the  $a$ -axis are a principal feature of the feldspar structure. These chains impose a linear pattern on faces  $(010)$  and  $(001)$  parallel to the  $a$ -axis. However, this linear arrangement does not affect the arrangement of tetrahedra on  $(110)$  and  $(20\bar{1})$ . The  $(010)$  and  $(001)$  growth faces are also parallel to planes of low bond density that cause preferred  $(010)$  and  $(001)$  feldspar cleavage. It is apparent that in all occurrences the crystal faces that accumulate abundant inclusions are those that

maintain the most constant and two-dimensionally isotropic bond density during growth. The mechanism for accumulation of inclusions, however, is still obscure.

*A case of post-magmatic sector-zoning: comparison with the Papoose Flat pluton.* Dickson (1968, and pers. comm.) found biotite inclusions beneath {110} in Papoose Flat orthoclase, as in the Godani microclines, but also found a greater abundance of plagioclase inclusions beneath {010} and {001}, unlike the Godani megacrysts. Moreover, his description and the author's observations indicate that there are no inclusions of apatite, sphene, or hornblende in the Papoose Flat megacrysts (though these minerals are found in the groundmass): in the Godani megacrysts all of the groundmass minerals bring out the pattern of sector-zoning.

Dickson (unpub. manuscript) proposes that the Papoose Flat megacrysts grew by post-magmatic replacement, and that the mineral inclusions exsolved from chemically different sectors. The small amount of biotite (< 1%, author's data) in the Papoose Flat megacrysts permits this conclusion. However, exsolution cannot explain the mineral inclusions of Godani megacrysts: 6-9% of the inclusion-rich rims are composed of biotite, hornblende, sphene, and apatite. Furthermore, the chemical composition of Godani megacrysts plus inclusions (Table II, p. M42) is unnaturally rich in Mg and Ti (ref. chemical data compiled by Smith, 1974). This minor element superabundance is most remarkable for Ti; Smith (1974) refers to no natural feldspar with > 0.37% TiO<sub>2</sub>, yet the Godani 'megacryst plus inclusion' analyses have up to 0.61% TiO<sub>2</sub>. This high amount of TiO<sub>2</sub> can be accounted for by inclusion of groundmass sphene, but cannot be attributed to exsolution from a Ti-rich K-feldspar.

The occurrence of sector-zoning at Papoose Flat, where sector-zoned megacrysts are found in quartzite wall rock, is different from the occurrence in the Godani Valley where the megacrysts are found only in the pluton. It is evident that the Papoose Flat megacrysts did not grow within magma, unlike the Godani Valley megacrysts. This difference points to the fact that superficially similar sector-zoning can occur in different ways.

*Conclusions.* Sectoral preference for inclusions in microcline megacrysts from the Godani Valley pluton is similar to features described by Schermerhorn (1956) and Piveç (1969) from European localities. Growth shapes of the Godani megacrysts show that accelerated growth of the {110} and {201} faces is associated with preference for inclusions on these surfaces. However, comparison with descriptions by Piveç and Schermerhorn indicates that growth rate is not the controlling

factor. The pattern of sector-zoning is due to crystallographic control of the acceptance of inclusions.

The previous descriptions by Schermerhorn and Piveç correlate this type of sector-zoning with a magmatic origin. Evidence for magmatic origin of the Godani megacrysts is provided by higher Ba concentrations in megacrysts than in groundmass microcline, by preservation of a monoclinic 131 powder diffraction peak in megacrysts near the pluton margins, indicating contact chilling of a magma, and by an absence of quartz inclusions in the megacryst rims. The disappearance of quartz inclusions during megacryst rim crystallization can be explained within the Ab-Or-An-Qz system by movement of the feldspar-quartz saturation surfaces towards the quartz apex with decrease in total pressure. Such a rapid decrease in pressure must be brought about by upward intrusion or de-gassing of a magmatic body.

One point mentioned in the text above is not yet resolved. This is the question of why the megacrysts at site 46 (fig. 1) lack sector-zoning. Aside from more complete re-equilibration of megacryst structural states, the only distinctive feature of site 46 is its great abundance of megacrysts (14% by volume). The next greatest abundance in the pluton is 11% by volume. The megacrysts at site 46 are not exceptionally large, they are just more abundant. The lack of sector-zoning at site 46 is apparently related to greater nucleation rate and more rapid growth of megacrysts at this site. For these reasons megacryst growth may have been complete at site 46 before the development of sector-zoned rims on megacrysts elsewhere in the pluton.

## REFERENCES

- Bahat (D.), 1974. *Am. Mineral.* **59**, 139-42.  
 Bence (A. E.) and Albee (A. L.), 1968. *J. Geol.* **76**, 382-403.  
 Carmichael (I. S. E.), 1963. *Q. J. Geol. Soc.* **119**, 95-131.  
 Dickson (F. W.), 1968. Abstr. in *Geol. Soc. Am. Ann. Meet.*, Mexico City, 74-5.  
 Evans (H. T.), Appleman (D. E.), and Handwerker (D. S.), 1963. Abstr. in *Am. Crystallogr. Assoc. Ann. Meet.*, Cambridge, 42-3.  
 Kastner (M.) and Waldbaum (D. R.), 1968. *Am. Mineral.* **53**, 1574-602.  
 Kerrick (D. M.), 1969. *Am. Mineral.* **54**, 839-48.  
 Laves (F.) and Goldsmith (J. R.), 1961. *Cursillos y Conferencias Inst. 'Lucas Mallada'*, **8**, 71-80.  
 Luth (W. C.), 1969. *Am. J. Sci.* **267A**, 325-41.  
 — Jahns (R. H.) and Tuttle (D. F.), 1964. *J. Geophys. Res.* **69**, 759-73.  
 Oftedal (I.), 1959. *Norsk Geol. Tidsskr.* **39**, 343-9.  
 Piveç (E.), 1969. *Acta Univ. Carol., ser. geol.*, **n. 1**, 11-25.



- Presnall (D. C.) and Bateman (P. C.), 1973. *Geol. Soc. Am. Bull.* **84**, 3181-202.
- Schermerhorn (L. J. G.), 1956. *Am. J. Sci.* **254**, 329-45.
- Smith (J. V.), 1974. *Feldspar Minerals*, **2**, Springer-Verlag, New York.
- Stewart (D. B.) and Wright (T. L.), 1974. *Bull. Soc. fr. Minéral. Crystallogr.* **97**, 356-77.
- Taylor (S. R.) and Heier (K. S.), 1960. *Int. Geol. Congress*, 21st session, **pt. 14**, 47-61.
- Wright (T. L.) and Stewart (D. B.), 1968. *Am. Mineral.* **53**, 38-87.

[Manuscript received 12 August 1977,  
revised 23 May 1978]

# Vaniman: Sector-zoned microcline megacrysts (App.) M41

## CRYSTALLIZATION HISTORY OF SECTOR-ZONED MICROCLINE MEGACRYSTS

### FROM THE GODANI VALLEY PLUTON, NIGERIA

David Vaniman

Board of Earth Sciences, University of California,  
Santa Cruz, California 95064 USA

THIS section briefly summarizes some chemical and crystallographic details of the Godani Valley pluton and sector-zoned microcline megacrysts. Table 1 lists microprobe data for unzoned groundmass microcline, and for microcline megacrysts by sector (core, inclusion - rich rim and inclusion - poor rim sectors). The analyses in table 1 are focused-beam (about 5 $\mu$ m) data that exclude coarse perthite exsolution and mineral inclusions.

Table 2 contains representative x-ray fluorescence analyses of the megacryst - free pluton groundmass and of the cores, inclusion - poor rims and inclusion - rich rims of two microcline megacrysts. Modal data are used to obtain the total rock compositions (groundmass plus megacrysts) plotted in figures 8 and 9.

### Powder Diffraction Cell Parameter Refinements

The powder diffraction methods of Wright and Stewart (1968) were used to make 45 determinations of tetrahedral site occupancy in eight megacrysts. Weissenberg and Buerger-precession photographs were taken of 23 fragments from these same eight specimens to examine diffraction symmetries within small portions of the megacrysts. The Al-Si distribution and diffraction symmetry show no systematic difference between megacryst sectors. If there were sectoral differences in symmetry or tetrahedral site occupancy they have been lost by sub-solidus re-equilibration.

There is a tendency for megacrysts which are not sector-zoned (those from site 46, fig. 1) to give better cell parameter refinements. Three out of six refinements for non - sector-zoned megacrysts were acceptable, whereas only one out of 49 refinements from sector-zoned megacrysts were acceptable. The four accepted refinements are shown in figure 10 on the b - c plot of Stewart and Wright (1974). Core and rim portions of a crystal from site 46 (non - sector-zoned) and the core of a crystal from site 51 (sector-zoned) plot near the a contour of 8.55 angstroms. Another core portion of the crystal from site 46 plots at an a dimension of about 8.46 angstroms; this analysis is anomalous in that the a dimension indicated by the contours in figure 10 is less than the a dimension of the cell parameter refinement (8.55 angstroms). This anomalously small a dimension is due to the strain involved in fine - scale perthitic exsolution (ref. Smith, 1961; Wright and Stewart, 1968; Robin, 1974).

Despite the difficulties in obtaining acceptable cell parameter refinements, the data indicate a high degree of Al-Si ordering in all of the megacrysts. The four accepted cell parameter refinements plot between 0.90 and 0.95 Al-Si ordering (fig. 10); all 45 refinements would plot between 0.95 and 1.00 Al-Si ordering. This high degree of Al-Si order is not accompanied by the triclinic x-ray diffraction symmetry that one would normally expect (see the section on "Mappable Variation in 131 - 131 Peak Separation within the Pluton", in the main body of the text).

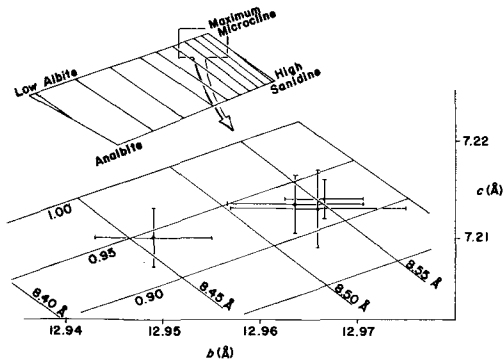


Fig. 10

Cell parameters of four megacryst samples plotted on the b - c diagram of Stewart and Wright (1974). The diagram is contoured for a (negative slope) and relative Al-Si ordering on an arbitrary scale of 0 to 1 (positive slope). Core and rim portions of one crystal (site 46) and a core portion of another (site 51) plot at the a contour of 8.55 angstroms. Another core portion from the crystal of site 46 plots with a strained a value of about 8.46 angstroms (calculated a = 8.55 angstroms). Bars extend to  $\pm 2$  standard error (Evans, Appleman and Handwerker, 1963 cell parameter refinement method).

**Acknowledgements** The help of Kenneth L. Cameron, Maryellen Cameron and Aaron Waters is greatly appreciated. Edwin Pivec of the Geological Survey of Czechoslovakia and F. W. Dickson of Stanford University kindly supplied specimens from other localities or unpublished data. Research was funded by Geological Society of America grant #1807-74, a Society of the Sigma Xi grant in aid of research, and the Chancellor's Patent Fund of the University of California.

I am especially grateful to Director C. N. Okozie and the officers of the Geological Survey of Nigeria for their assistance and incomparable kindness.

Table 1 Representative Electron Microprobe Analyses of Sector-zoned Megacrysts and Groundmass Microcline

	Megacryst Cores			Inclusion-rich Megacryst Rims			Inclusion-poor Megacryst Rims			Groundmass Microcline								
	2c*	20c	46c	51c	57c	18 av. of anal.	21	20i	51i	57i	19 av. of anal.	2g	20g	46g	51g	57g	av. of anal.	S.D.
SiO <sub>2</sub>	64.71	64.36	64.90	64.39	64.39	64.61	64.61	64.61	64.61	64.61	64.50	64.45	64.62	64.72	64.73	64.52	64.66	0.16
TiO <sub>2</sub>	0.06	0.05	0.00	n.a.	0.07	0.04	0.02	0.04	0.05	0.04	0.03	0.04	0.05	0.00	n.a.	0.04	0.03	0.02
Al <sub>2</sub> O <sub>3</sub>	18.37	18.71	18.24	18.41	18.54	18.42	18.30	18.41	18.67	18.74	18.54	18.45	18.36	18.43	18.48	18.20	18.36	0.12
FeO	0.22	0.14	0.07	0.04	0.11	0.11	0.06	0.13	0.11	0.06	0.13	0.13	0.05	0.12	0.12	0.03	0.08	0.11
MgO	0.10	0.10	0.04	0.06	0.12	0.08	0.03	0.10	0.08	0.05	0.10	0.08	0.02	0.11	0.10	0.04	0.10	0.08
BaO	0.96	1.06	1.00	1.16	1.01	0.97	0.14	0.72	0.71	0.79	1.45	0.90	0.28	0.80	0.76	0.80	0.94	0.80
CaO	0.01	0.00	0.00	0.01	0.00	0.01	0.01	0.00	0.01	0.01	0.02	0.01	0.01	0.01	0.02	0.01	0.02	0.01
Na <sub>2</sub> O	0.73	0.95	0.76	0.76	0.82	0.80	0.11	1.03	0.70	0.76	0.95	0.89	0.13	0.96	1.06	0.55	0.87	0.88
K <sub>2</sub> O	15.29	15.00	15.06	15.03	15.19	15.17	0.17	14.87	15.51	15.24	14.78	15.09	0.26	15.09	15.68	15.73	15.82	15.81
sum	100.45	100.37	100.09	99.86	100.25	100.21		99.88	100.45	100.46	100.24	100.24		99.81	100.43	100.50	100.20	100.10
Ab	6.58	8.60	7.17	6.97	7.43	7.28	1.01	9.39	6.34	6.94	8.64	8.08	1.17	8.69	9.59	7.88	7.99	1.46
An	0.05	0.00	0.00	0.07	0.00	0.06	0.03	0.00	0.00	0.00	0.11	0.06	0.05	0.06	0.10	0.06	0.05	0.04
mol.% Or	91.58	89.49	91.01	90.85	90.74	90.91	1.23	89.31	92.40	91.62	88.62	90.23	1.49	89.82	88.93	93.46	90.38	90.52
Ch	1.89	1.91	1.82	2.11	1.83	1.75	0.26	1.30	1.26	1.44	2.63	1.63	0.50	1.43	1.38	1.45	1.69	1.43
*Numbers refer to sample localities of fig. 1; suffixes c = megacryst core, i = inclusion-rich megacryst rim, l = inclusion-poor megacryst rim, g = groundmass microcline																		
†Total Fe as FeO																		

Table 2: Representative X-ray Fluorescence Analyses

	Groundmass Analyses <sup>a</sup>										Megacryst Analyses				
	2*	4	7	16	45	46	47	52	53	20c <sup>†</sup>	20i	20I	7c	7i	7I
SiO <sub>2</sub>	69.33	68.41	70.22	68.15	68.57	68.88	69.43	69.96	67.82	64.13	62.93	61.35	65.48	63.50	62.83
TiO <sub>2</sub>	0.37	0.61	0.43	0.57	0.44	0.53	0.50	0.44	0.60	0.23	0.47	0.61	0.39	0.33	0.54
Al <sub>2</sub> O <sub>3</sub>	15.73	14.87	14.60	14.86	15.72	14.51	14.79	14.82	15.22	17.31	18.52	17.96	17.06	18.62	18.07
<sup>†</sup> Fe <sub>2</sub> O <sub>3</sub>	0.63	0.93	0.73	1.07	0.69	1.01	0.77	0.75	0.91	0.10	0.12	0.33	0.24	0.12	0.24
FeO	1.67	2.45	1.92	2.84	1.85	2.66	2.06	1.98	2.41	0.27	0.30	0.86	0.66	0.30	0.69
MnO	0.03	0.04	0.03	0.04	0.03	0.05	0.03	0.03	0.04	0.00	0.01	0.02	0.01	0.00	0.01
MgO	1.08	1.53	1.26	1.51	1.26	1.86	1.28	1.13	1.52	0.20	0.20	0.58	0.44	0.21	0.48
CaO	2.63	3.22	2.89	3.07	3.07	3.30	3.09	2.70	3.16	0.54	1.00	1.32	0.81	0.64	0.96
Na <sub>2</sub> O	4.69	4.41	4.68	4.36	4.67	4.30	4.33	4.49		2.13	2.43	2.24	2.04	2.13	1.98
K <sub>2</sub> O	3.78	3.07	2.60	3.11	2.83	2.20	2.94	3.50	3.05	11.76	12.02	11.42	11.45	12.47	12.36
P <sub>2</sub> O <sub>5</sub>	0.11	0.18	0.12	0.16	0.12	0.15	0.13	0.14	0.17	0.06	0.07	0.07	0.09	0.06	0.07
BaO	0.24	0.22	n.a.	0.20	0.20	0.18	0.21	0.21	0.21	0.65	0.61	n.a.	0.59	0.65	0.63
LOI	0.30	0.39	0.52	0.48	0.80	0.70	0.60	0.63	0.54	2.23	1.62	2.80	1.08	1.37	1.67
sum	100.59	100.33	100.00	100.42	100.25	100.33	100.16	100.62	100.14	99.61	100.30	99.56	100.34	100.40	100.53
Rb(ppm)	150	170	n.a.	135	110	125	128	145	110	249	247	n.a.	255	269	265
Sr(ppm)	748	625	n.a.	860	700	700	680	555	705	1021	976	n.a.	950	1074	1017
qr	20.17	21.84	24.89	21.59	21.75	25.01	24.33	23.73	20.81	5.45	0.65	1.11	7.52	1.88	1.47
or	22.34	18.14	15.36	18.38	16.72	13.00	17.37	20.68	18.02	69.49	71.03	66.01	67.66	73.69	73.04
ab	39.69	37.32	39.60	36.89	39.52	36.39	36.64	36.64	37.99	18.02	20.56	18.53	17.26	18.02	16.75
an	10.71	11.71	11.15	11.79	13.57	13.79	12.24	10.67	12.37	2.29	4.03	5.10	3.43	2.76	3.92
di	1.33	2.52	1.96	1.97	0.71	1.30	1.83	1.49	1.80	0.00	0.00	0.67	0.00	0.00	0.31
ky	3.86	5.13	4.25	4.95	6.75	6.99	4.45	6.22	5.42	0.50	0.10	1.35	1.40	0.52	1.17
mt	1.01	1.49	1.17	1.73	1.12	1.62	1.25	1.20	1.46	0.16	0.00	0.51	0.39	0.00	0.39
il	0.70	1.16	0.82	1.08	0.84	1.01	0.95	0.84	1.14	0.44	0.33	1.14	0.74	0.61	1.03
ap	0.25	0.42	0.28	0.37	0.28	0.35	0.30	0.32	0.39	0.14	0.16	0.16	0.21	0.14	0.16

\*column headings refer to sample localities of fig. 1

<sup>†</sup>suffixes for megacryst portions used as in table 2

<sup>†</sup>Fe<sub>2</sub>O<sub>3</sub>/FeO ratio is based on Fe<sup>+++</sup>/Fe<sup>++</sup> ratio (0.34) of a rock sample from the Godani pluton analyzed by C.C. Patel of the Geological Survey of Nigeria (wet chemical analysis)

<sup>†</sup>% weight loss on ignition at 1000°C

<sup>†</sup>wt.% megacrysts in outcrop: 2(11.3%), 4(4.0%), 7(10.6%), 16(2.5%), 45(11.3%), 46(13.2%), 47(3.7%), 52(7.0%), 53(5.4%)

## Hall: Pyroxenes from an ophiolite mélangé

### PYROXENES OF BASIC ROCKS AND RODINGITES FROM AN OPHIOLITE MÉLANGÉ,

#### SOUTH-EASTERN TURKEY

Robert Hall

Department of Geology, Queen Mary College,

London University, London E1 4NS

THE Taurus fold-belt is the southernmost of the two major fold-belts forming the Anatolian sector of the Alpine-Himalayan mountain chain. The interior of the Eastern Taurus is occupied by an extensive area of largely pre-Permian metamorphic rocks known as the Bitlis Massif. This is thrust southward over an ophiolite-flysch complex which is in turn thrust southward over sedimentary rocks of the Arabian foreland. The ophiolite-flysch complex is part of a zone of Tethyan ophiolites that occurs discontinuously throughout the Middle East between Cyprus and Oman (the 'Crescent Ophiolite Peri-Arab' of Ricou, 1971). At the southern margin of the Bitlis Massif near the village of Mutki ophiolites occur as a tectonic mélangé which consists of blocks of basic volcanics, gabbros and picrites, radiolarian cherts and other minor sedimentary components, serpentinites and podiform chromite bodies, together with rodingites and silicon-carbonate rocks. All of these blocks are incorporated in a matrix of serpentinite (Hall, 1976).

Pyroxenes are common in the basic rocks of the mélangé. Textural evidence suggests that most of them are of igneous origin, despite the complex thermal and structural history of the mélangé, which includes several episodes of tectonic mixing, metamorphism and metasomatism. Recent work indicates that igneous clinopyroxene may survive metamorphism, without re-equilibration, under conditions of the greenschist facies (Wallace, 1974, 1975) and glaucophane-lawsonite-schist facies (Schubert and Seidel, 1972; Mevel and Velde, 1976) and therefore microprobe analyses were made to determine if the pyroxene chemistry is consistent with an igneous origin or if there have been changes due to metamorphism and metasomatism.

#### Petrography of the tectonic blocks

Volcanic rocks occur in the mélangé in blocks several kilometres across which have been metamorphosed and deformed and are marginally recrystallised as greenschists or crossite-bearing schists. The greenschists contain assemblages typical of the greenschist facies except for the amphibole which microprobe analysis indicates is hornblende rather than actinolite. Crossite partly replaces hornblende in some greenschists, and is the only amphibole in the crossite-bearing schists. The appearance of either crossite or hornblende seems to be controlled by the bulk-rock Fe<sub>2</sub>O<sub>3</sub>/FeO ratio, as shown by Ernst et al. (1970) for similar rocks from the Santagawa terrain. The cores of the blocks are meta-basalts, interbedded with radiolarian cherts, which frequently have agglomeratic textures and contain both lithic and mineral fragments. Mineral assemblages in the meta-basalts are clinopyroxene + albite + chlorite + sphene + opaque ± crossite. The petrography and mineralogy of the volcanic rocks (Hall, 1974) suggests that they have been metamorphosed under conditions trans-

sitional between the glaucophane-lawsonite schist facies and the greenschist or greenschist-amphibolite transitional facies of Turner (1968). Metamorphic pyroxenes crystallised under these conditions are likely to be green sodic pyroxenes with compositions between omphacite and aegirine-augite (Essene and Fyfe, 1976; Brown, 1974; Newton and Fyfe, 1976). In one meta-basalt a green clinopyroxene, whose optical properties indicate aegirine-augite, occurs in a cavity as sub-idioblastic elongate prisms intergrown with albite and an opaque phase. This pyroxene is interpreted as metamorphic in origin. All the other clinopyroxenes in the meta-basalts appear to be igneous relics. Colourless euhedral phenocrysts up to 2 mm in length occur both in and between lithic fragments, often with a groundmass of pink granular pyroxene. Crossite, when present, nucleates on the clinopyroxene, and epidote, actinolite and carbonate occur as late metamorphic vein-filling phases.

Gabbros and picrites occur as blocks usually less than three hundred metres across. The picrites often have a marked mineralogical layering, and consist of cumulus olivine, with clinopyroxene and plagioclase as intercumulus phases. Orthopyroxene occurs in some samples. These rocks have escaped any significant metamorphism; olivine is partly serpentinised, but the pyroxenes are generally quite fresh. The gabbros have been metamorphosed, but under different conditions to those prevailing during the metamorphism of the volcanic rocks. They are partially altered to actinolite + chlorite + albite assemblages; plagioclase is always altered, but usually a relict igneous texture is preserved, often with clinopyroxene. Olivine (F<sub>0</sub>) occurs in one sample. Where completely recrystallised, assemblages are typical of the greenschist facies, and in contrast to the meta-volcanics crossite is absent, while actinolite rather than hornblende is the characteristic amphibole. In addition, the gabbros and picrites always show some signs of calcium metasomatism while the meta-volcanics do not. In the picrites and many of the gabbros this metasomatism has resulted in an alteration of the original plagioclase to a fine-grained intergrowth of grossular, prehnite and clinozoisite. In some blocks alteration is more extensive and clinopyroxene may coexist with such minerals as grossular, prehnite, and idocrase. Although these rocks often have a gabbroic appearance, and correspond to the 'rodingites' of some authors (see review by Coleman, 1967) it is difficult to be certain if the clinopyroxene is a relict igneous phase, or is of metasomatic origin. This problem is complicated because these rocks almost always show some signs of cataclasis, and may be extensively mylonitised.

#### Pyroxene compositions

Eight rocks containing clinopyroxene were selected for study: two meta-basalts (RM9, RM290), two gabbros (RM116, RM203), two rodingites (RM228, RM17) and two picrites (RM5, RM19). Each sample is from a separate block in the mélangé. Mineral analyses were made using the Microscan V microprobe at University College London, operated at an accelerating voltage of 20 kV with a specimen current of approximately 2 × 10<sup>-8</sup> amp. All pyroxenes were analysed for Si, Ti, Al, Fe, Mn, Mg, Ca, Na, K and Cr. Pure metal standards were used for Ti, Mn and Cr, and natural silicate standards for the other elements. The raw data were reduced using the EM-10-NPL computer programme (Wason et al., 1969).

The compositions and structural formulae of the analysed pyroxenes are presented in Tables 1 to 3. None of the pyroxenes was zoned with respect to Ca, Mg or Fe, and with the exception of groundmass pyroxenes from meta-basalt RM290, and rodingite RM17 which contains two chemically distinct clinopyroxenes, there is very little compositional variation between different grains in the same rock (Fig. 1).